AIAA JOURNAL
Vol. 30, No. 8, August 1992

Explicit Runge-Kutta Method for Three-Dimensional Internal Incompressible Flows

H. Cabuk*
Columbia University, New York, New York 10027
C.-H. Sung†
David Taylor Research Center, Bethesda, Maryland 20084
and
V. Modi‡
Columbia University, New York, New York 10027

A computer code has been developed to obtain the steady-state solutions for three-dimensional laminar incompressible flow governed by the Navier-Stokes equations. A central difference finite-volume formulation with an explicit one-step multistage Runge-Kutta time-stepping scheme for the primitive variables (i.e., velocity components and pressure) is used. The preconditioning matrix method, which is a generalized version of the artificial compressibility method, is used to construct a pressure equation from the continuity equation. Fourth-order artificial dissipation is used to suppress high-frequency oscillations. Numerical techniques to accelerate the rate of convergence include local time stepping and implicit residual smoothing. The code is validated by determining its ability to accurately predict 1) boundary-layer growth in a square duct with established and entry flow upstream conditions, 2) secondary flow in a 90-deg bend of a square cross section, and 3) separation and reattachment in flow over a backward-facing step. The calculations are found to compare favorably with experimental data and numerical calculations available in the literature.

Introduction

OUR interest was in solving internal flow problems in domains with curved boundaries. It was desired that the method be able to model the following flow features with adequate accuracy: boundary-layer growth along a wall, secondary flow effects that accompany flow turning, and flow separation. In the present study, laminar internal flows at Reynolds numbers <800 have been considered. The method has been successfully applied by Sung[1] to turbulent external flows at Reynolds numbers of the order of 10^6.

One of the main difficulties associated with the solution of the incompressible Navier-Stokes equations in a velocity-pressure formulation is the lack of a time evolution equation for pressure. If only steady-state solutions are of interest, this difficulty can be overcome by using the so-called artificial compressibility method. This method has been introduced independently and under slightly different forms by other researchers.[2,3] A generalized version of the artificial compressibility method the so-called preconditioned matrix method, developed by Turkel,[4] has been adopted here. A similar approach for inviscid incompressible flow has also been suggested by Rizzi and Eriksson.[5]

An explicit one-step multistage Runge-Kutta stepping scheme is used for integration in time. The use of explicit Runge-Kutta methods as time-stepping schemes for the solutions of the compressible Euler equations has become popular since the appearance of papers by Jameson et al.[6] and Rizzi and Eriksson.[7] This approach has been extended to the compressible Navier-Stokes equations by several investigators.[8-11] Rizzi and Eriksson[5] have extended this method to inviscid incompressible flow, and Sung[12] has extended the method to incompressible turbulent flows. Implicit schemes have less restrictive stability requirements than explicit schemes but require more extensive calculations to such a degree that their use may compensate the gain in a larger stability limit. The severe stability restriction of the conventional explicit methods is relaxed by the enlarged stability region of Runge-Kutta methods. The four-stage Runge-Kutta time-stepping scheme used by Sung[12] is first order accurate in time and has a hyperbolic stability limit of 3. Here this method has been chosen because of its higher stability limit since only steady-state solutions are of interest and time accuracy is not an issue.

Local time stepping is used to accelerate the rate of convergence. A fourth difference, linear artificial dissipation, is introduced to damp high-frequency oscillations, and an implicit residual scheme is used to increase the stability limit of the method.

In the case of entry flow the boundary-layer growth along the walls and the velocities along the centerline have been predicted accurately, compared to the experimental results of Goldstein and Kreid[13] and Beavers et al.[14] Second, the flow in a 90-deg bend with a square cross section has been solved. The velocities at different streamline locations have been compared with the experimental data of Taylor et al.[15] Finally, a two-dimensional backward-facing step flow has been investigated at different Reynolds numbers. The reattachment point

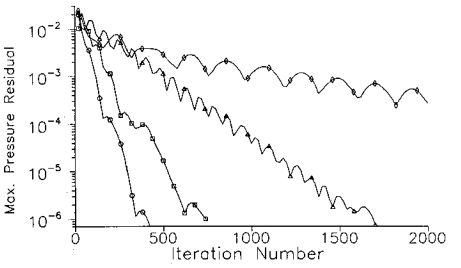

Fig. 1 Maximum pressure residuals vs iteration history for two-dimensional entry flow ($Re = 50$): ○, grid size 11×6; □, grid size 21×11; Δ, grid size 41×21; ◇, grid size 81×41.

Received May 13, 1991; revision received Oct. 7, 1991; accepted for publication Feb. 10, 1992.

*Postdoctoral Research Fellow, Department of Mechanical Engineering.

†Naval Architect. Member AIAA.

‡Assistant Professor, Department of Mechanical Engineering. Member AIAA.

of the separated region is compared with the experimental and numerical results of Armaly et al. [16] and the numerical results of Ku et al.[17]

Description of Numerical Method

The conservative form of the unsteady incompressible nondimensional continuity and Navier-Stokes equations are

$$u_{i,t} + (u_j u_i)_{,j} = -p_{,i} + Re^{-1} u_{i,jj}$$

$$u_{i,i} = 0 \tag{1}$$

The variables have been nondimensionalized by the mean velocity at the duct entrance, V, and by a characteristic length of the geometry, L, in the following manner: the velocities u_i, by V, the space coordinates x_i, by L, pressure by ρV^2, and time by L/V. The Reynolds number in Eqs. (1) is given by $Re = VL/\nu$. The derivations in the following sections are given for nondimensional variables. The preconditioned three-dimensional incompressible Navier-Stokes equations are then given by

$$Eq_t + F_x + G_y + H_z = 0 \text{ or } q_t + E^{-1}(F_x + G_y + H_z) = 0 \tag{2}$$

where the subscripts are partial derivatives with respect to the time t and the three Cartesian coordinates x, y, and z. The preconditioning matrix E and the column vectors of the variable q and of the three components of fluxes F, G, and H are defined as

$$E = \begin{bmatrix} \beta^{-2} & 0 & 0 & 0 \\ \gamma u & 1 & 0 & 0 \\ \gamma v & 0 & 1 & 0 \\ \gamma w & 0 & 0 & 1 \end{bmatrix}, \quad E^{-1} = \begin{bmatrix} \beta^2 & 0 & 0 & 0 \\ -\gamma u & 1 & 0 & 0 \\ -\gamma v & 0 & 1 & 0 \\ -\gamma w & 0 & 0 & 1 \end{bmatrix}$$

$$q = \begin{bmatrix} p \\ u \\ v \\ w \end{bmatrix}, \quad F = \begin{bmatrix} u \\ u^2 + p - \tau_{xx} \\ uv - \tau_{xy} \\ uw - \tau_{xz} \end{bmatrix}$$

$$G = \begin{bmatrix} v \\ vu - \tau_{yx} \\ v^2 + p - \tau_{yy} \\ vw - \tau_{yz} \end{bmatrix}, \quad H = \begin{bmatrix} w \\ wu - \tau_{zx} \\ wv - \tau_{zy} \\ w^2 + p - \tau_{zz} \end{bmatrix}$$

where p is the pressure; u, v, and w are the three Cartesian components of the velocity; and the stresses are defined as

$$\tau_{ij} = Re^{-1}(u_{i,j} + u_{j,i}), \qquad i,j = 1, 2, 3$$

where $(u_1, u_2, u_3) = (u, v, w)$, and $(x_1, x_2, x_3) = (x, y, z)$. The symbols γ and β represent preconditioning parameters. The idea is to choose β^2 for a given γ so that disparity in propagating speeds of the acoustic and convective waves is reduced during the transient state. The fact that the transient-state solution is not physically valid is irrelevant since only the steady-state solution is of interest. Neglecting the viscous terms, Eq. (2) is rewritten as

$$q_t + Aq_x + Bq_y + Cq_z = 0 \tag{3}$$

where

$$A = \begin{bmatrix} 0 & \beta^2 & 0 & 0 \\ 1 & (2-\gamma)u & 0 & 0 \\ 0 & (1-\gamma)v & u & 0 \\ 0 & (1-\gamma)w & 0 & u \end{bmatrix}$$

$$B = \begin{bmatrix} 0 & 0 & \beta^2 & 0 \\ 0 & v & (1-\gamma)u & 0 \\ 1 & 0 & (2-\gamma)v & 0 \\ 0 & 0 & (1-\gamma)w & v \end{bmatrix}$$

$$C = \begin{bmatrix} 0 & 0 & 0 & \beta^2 \\ 0 & w & 0 & (1-\gamma)u \\ 0 & 0 & w & (1-\gamma)v \\ 1 & 0 & 0 & (2-\gamma)w \end{bmatrix}$$

To derive the eigenvalues, Eq. (3) is Fourier transformed to give

$$D = \omega_1 A + \omega_2 B + \omega_3 C \tag{4}$$

where the absolute values of Fourier components ω_1, ω_2, and ω_3 are bounded by 1. It is found that

$$\lambda_{1,2} = U$$

$$\lambda_{3,4} = \frac{1}{2}\left[(2-\gamma)U \pm \sqrt{(2-\gamma)^2 U^2 + 4\beta^2(\omega_1^2 + \omega_2^2 + \omega_3^2)}\right] \tag{5}$$

where $U = \omega_1 u + \omega_2 v + \omega_3 w$. Minimization of the minimum of the ratios of the eigenvalues in Eq. (5) gives the condition for the choice of β^2 for a given γ (see Ref. 4) as

$$\beta^2 = \{1 + |2-\gamma|\}\hat{U}^2 \tag{6}$$

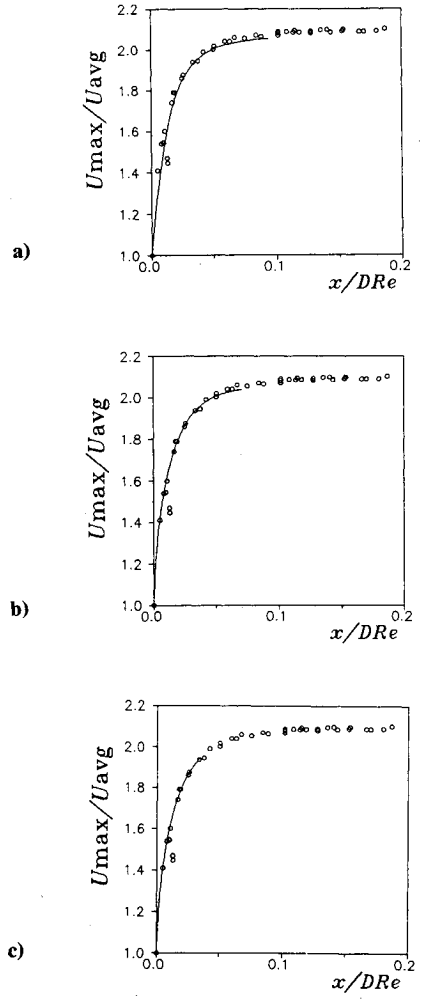

Fig. 2 Streamwise velocity development along the duct centerline: solid line, computations; circles, data from Ref. 13. a) $Re = 32$, b) $Re = 100$, and c) $Re = 100$ (shorter computational domain).

where $\hat{U} = |u| + |v| + |w|$. The optimum choice of the preconditioning parameters, according to this criterion, are $\gamma = 2$ and the $\beta^2 = \hat{U}^2$, which suggests that β^2 be determined locally as recommended in reference by Rizzi and Eriksson.[5] They recommend β^2 to be proportional to the local velocity squared, i.e.,

$$\beta^2 = \max[0.3, r(u^2 + v^2 + w^2)] \tag{7}$$

where r is a constant in the range $1 < r < 5$. Numerical experiments indicate that $\gamma = 0$ and $\beta^2 = 1$, a choice that corresponds to a pure artificial compressibility method, provides a reasonably good convergence rate.

Spatial discretization is done using a finite-volume formulation with the dependent variables defined at the center of a computational cell, and the fluxes evaluated at the midpoint of each cell face to produce central differences. A set of first-order ordinary differential equations in the semidiscrete form

$$\frac{dq}{dt} = Q(q) \tag{8}$$

is then obtained.

Because of the use of the central difference scheme, which is unconditionally unstable to strongly advective flows, artificial dissipation is needed to damp high-frequency oscillations. Here a fourth-order linear artificial dissipation term is used. With the addition of the artificial dissipation terms, Eq. (8) can be written as

$$\frac{dq}{dt} = Q(q) - D(q) = R(q) \tag{9}$$

where

$$D(q) = \epsilon \cdot K \cdot \left(\frac{\partial^4 q}{\partial \xi^4} + \frac{\partial^4 q}{\partial \eta^4} + \frac{\partial^4 q}{\partial \zeta^4} \right) \tag{10}$$

and $\epsilon = 0.05$, and K is given by

$$K = \tanh(\Delta V / \Delta V_{\max})$$

where ΔV is the cell volume in curvilinear coordinates (ξ, η, ζ) and $\Delta V_{\max}$ is the maximum cell volume.

The resulting set of ordinary differential equations can now be integrated in time using any time-stepping scheme until steady state is reached. In this paper a Runge-Kutta scheme has been used. Explicit one-step time-stepping schemes of Eq. (9) can be expressed as

$$q^{(n+1)} = S(\Delta t J) q^n \tag{11}$$

where J is the Jacobian of R, the right-hand side of (9), and S is a polynomial of degree m in the matrix $z = \Delta t J$:

$$S(z) = 1 + z + \beta_2 z^2 + \beta_3 z^3 + \cdots + \beta_m z^m \tag{12}$$

It is noted that m is the number of functional evaluations and is also called the number of Runge-Kutta stages. The stability region of Eq. (11) is defined as $S = \{z : |S(z)| \le 1\}$. For J having imaginary eigenvalues λ (i.e., hyperbolic systems), the maximum stability limit is at the boundary S_1 at the intersection of the stability region S and the imaginary axis. Then the time-stepping scheme is stable if the time step size is chosen as

$$\Delta t = \frac{S_1}{\max(\lambda)} = \frac{CFL}{\max(\lambda)} \tag{13}$$

where S_1 is identified as the Courant-Friedrichs-Lewy (CFL) number. More detailed discussion of Runge-Kutta schemes are given by van der Houwen.[18]

The scheme used by Jameson et al.,[6]

$$S(z) = 1 + z + (1/2)z^2 + (1/6)z^3 + (1/24)z^4 \tag{14}$$

is fourth-order accurate with CFL = $2\sqrt{2}$, and the scheme used by Rizzi and Eriksson,[7]

$$S(z) = 1 + z + (1/2)z^2 + (1/2)z^3 \tag{15}$$

is second-order accurate with CFL = 2. The scheme used in this paper,

$$S(z) = 1 + z + (5/9)z^2 + (4/27)z^3 + (4/81)z^4 \tag{16}$$

is first order accurate with CFL = 3. For first-order-accurate schemes such as Eq. (16), the stability limit is CFL = $m - 1$, and one is tempted to think that schemes with a higher number of stages may be more efficient since a larger time step can be used. This turns out not to be true because a larger m also implies that more functional evaluations are required to forward one time step. Numerical experiments indicate that four to six stages seem to be the most efficient. Similar conclusion has also been arrived at by Pike and Roe[19] based on two-dimensional calculations.

To determine the time step size using stability criterion (13), the eigenvalues of Eq. (9) must be found. If both the viscous and artificial dissipation terms are neglected, then an estimate of the local time step based on hyperbolic equations for the stability requirement is obtained in the form

$$\Delta t \le \mathrm{CFL}\left(\frac{\Delta V}{\lambda_0} \right) \tag{17}$$

where λ_0 is the maximum of the eigenvalues given by Eq. (5) and ΔV is the cell volume. A direct application of this time step to the Navier-Stokes equations leads to an overestimate of the time step size, especially near the walls where viscous terms dominate, and may result in oscillations or even divergence. Swanson and Turkel[20] analyzed an unconditionally stable difference scheme used by Crocco[21] for a simple heat equation and gave an estimate of the time step that includes the viscous effect. A three-dimensional version of their estimate can be expressed as

$$\Delta t \le \frac{1}{\Delta t_H^{-1} + 2Re^{-1}(g^{11} + g^{22} + g^{33})} \tag{18}$$

where Δt_H is based on the inviscid model such as that given by Eq. (17), $g^{ii} = g^i \cdot g^i$, and g^i is the contravariant basis vector in

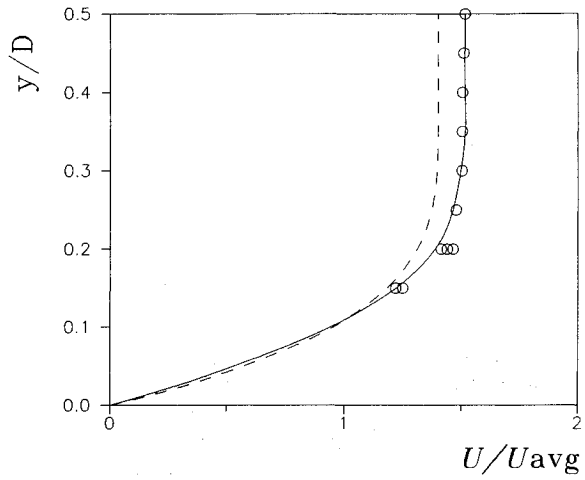

Fig. 3 Streamwise velocity profile at $x/(DRe) = 0.0075$: solid curve, $Re = 100$; dashed curve, $Re = 32$; circles, experimental data from Ref. 13.

the i direction. An alternative approach can also be derived. The eigenvalues of the Eq. (9) are complex valued. Substituting λ_0 of Eq. (17) with the magnitude of the largest eigenvalue of Eq. (9), one obtains an estimate of the time step as

$$\Delta t \leq \frac{\text{CFL}}{\lambda_H + 4Re^{-1}(g^{11} + g^{22} + g^{33}) + 48\epsilon K} \tag{19}$$

where $\lambda_H = \lambda_0/\Delta V$ and λ_0 is the maximum of the eigenvalues given by Eq. (5). Note that, if the artificial dissipation term is neglected, then Eqs. (18) and (19) are identical when CFL = 2. Numerical experiments indicate that the use of Eq. (19) exhibits somewhat better convergence properties than the use of Eq. (18) for the time step.

Another numerical technique incorporated into the scheme is the implicit residual smoothing. The mathematical motivation for using the residual smoothing technique is to reduce the spectral radius of the function on the right-hand side of an equation such as Eq. (9), thus enhancing the stability limit of the scheme. Following Jameson,[22] an implicit residual smoothing scheme is

$$(1 - \epsilon_\xi \delta_\xi^2)(1 - \epsilon_\eta \delta_\eta^2)(1 - \epsilon_\zeta \delta_\zeta^2)\hat{R}_{ijk} = R_{ijk} \tag{20}$$

where δ_ξ^2, δ_η^2, and δ_ζ^2 are second central differences; R_{ijk} is the unsmoothed residual; $\hat{R}_{ijk}$ is the smoothed residual to be used in the time integrations, and ϵ_ξ, ϵ_η, and ϵ_ζ are the smoothing parameters. This scheme has been implemented using the smoothing parameters $\epsilon_\xi = \epsilon_\eta = \epsilon_\zeta = 0.5$. Zero Dirichlet boundary conditions are used for the smoothed residuals.

The boundary conditions used for the internal flow simulation are discussed briefly in this section. Implementation of the velocity boundary conditions on the walls and on the symmetry planes is straightforward. At the entrance of the duct, the velocity component normal to the inlet is specified. For the remaining velocity components at the entrance, either zero normal derivative or zero velocity component can be specified. From a physical point of view, it is not clear what type of boundary conditions should be used at the entrance for the remaining velocity components. Numerical experiments have shown that specifying Neumann boundary conditions increases the rate of convergence significantly. The flow at the exit of the duct is not known a priori and is somewhat affected by what happens beyond the exit region. The proper way of handling this problem would be to extend the domain and specify suitable boundary conditions for the extended domain, i.e., some kind of infinity boundary conditions. In this paper zero normal derivatives for the velocity components have been prescribed. This is both mathematically acceptable and physically not so restrictive a choice.

In the literature a Neumann boundary condition for the pressure derived from the momentum equation normal to the boundary is usually enforced. In this research, except for the symmetry planes, pressure on the boundaries is extrapolated from the interior of the domain with zero second derivative on the boundary. This is a computational boundary condition for pressure and is suitable for internal flows because in internal flows the pressure at each cross section tends to be uniform with an approximately constant pressure gradient along the streamwise direction of the flow. For the symmetry planes zero normal derivative for pressure has been prescribed.

Numerical Results

The numerical code has been tested to determine its ability to accurately predict flow in different internal geometries. In the numerical calculations, pressure at one point in the domain is fixed. First, some preliminary tests have been carried out in relatively simple geometries to study the accuracy of the algorithm and the effect of grid size. Then entry flow in a square cross-sectional duct, flow in a 90-deg bend of square cross section, and flow over a backward-facing step have been investigated. The results of these tests have been compared with the experimental data available in the literature.

Preliminary Tests

Two-dimensional entry flow in a straight channel has been solved for a Reynolds number of 50 with different grid sizes (11×6, 21×11, 41×21, and 81×41). The length of the channel was twice the entrance length, and convergence criterion was 10^{-6} for the minimum residual. Other parameters chosen for this problem are

Artificial dissipation coefficient: $\epsilon = 0.05$
CFL number: CFL = 2.0
Sound speed: $\beta^2 = 2.0$
Implicit residual smoothing coefficients: $\epsilon_\xi = \epsilon_\eta = 0.5$

At the entrance a plug flow profile is specified for the normal velocity component. Other boundary conditions were same as those described in the preceding section. Established flow in the same geometry with an identical grid size is also computed. For this case an established velocity profile at the entrance is specified for the normal velocity component.

Both the problem of entry flow and established flow in a circular duct have been solved by using the axisymmetric version of the code with the following grid sizes: 11×6,

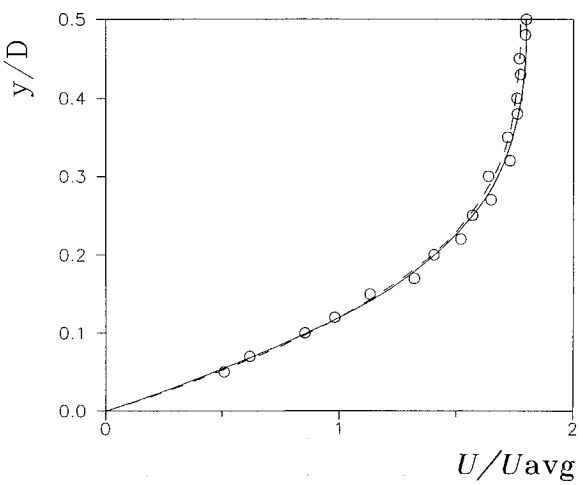

Fig. 4 Streamwise velocity profile at $x/(DRe) = 0.02$: solid curve, $Re = 100$; dashed curve, $Re = 32$; circles, experimental data from Ref. 13.

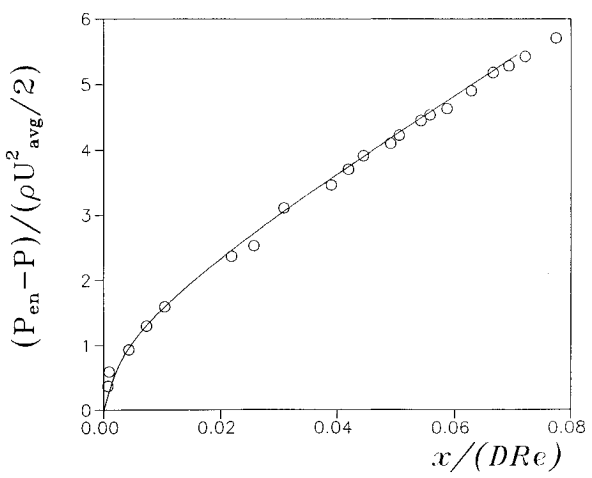

Fig. 5 Variation of the average pressure with $x/(DRe)$, where $Re = 100$. Solid line, computations; circles, data from Ref. 14.

Table 1 Predicted pressure gradients and corresponding relative errors

	Two-dimensional channel		Circular duct	
Grid	$(\partial p/\partial x)$	Error	$(\partial p/\partial x)$	Error
11×6	0.2523	5.1%	0.2778	15.7%
21×11	0.2422	0.9%	0.2474	3.1%
41×21	0.2404	0.15%	0.2410	0.4%
81×41	0.2401	0.02%	—	—
Exact	0.2400	—	0.2400	—

Table 2 Test runs for β^2 and $\gamma(U^2 = u_i u_i)$

Case no.	β^2	γ	No. of steps
1	max $(1.41U^2, 0.4)$	2.0	1200
2	max $(1.41U^2, 0.4)$	0.0	2800
3	max $(3U^2, 0.4)$	2.0	1600
4	max $(3U^2, 0.4)$	0.0	1600
5	1.0	0.0	3000
6	3.0	0.0	1200
7	3.0	2.0	1400

21×11, and 41×21. In this case the length of the duct was twice the diameter of the duct and Reynolds number was 100. The main reason for these tests was to study the accuracy of the solutions and convergence history of the code with varying grid size.

In both two-dimensional and axisymmetric established flows, the same flow profile at each cross section and a constant pressure gradient along the streamwise direction are obtained. In Table 1 predicted pressure gradients and relative errors are given for different grid sizes. In Fig. 1 the maximum pressure residual vs iteration history is given for different grids for a two-dimensional entry flow. With finer grids the number of iterations for convergence is found to increase. Qualitatively similar residual histories are obtained for the other cases (i.e., established flow in the two-dimensional channel and in the circular duct and entry flow in the circular duct). The pressure gradient obtained from a 21×11 grid is within 1% of the exact value, suggesting that this grid is close to an optimum grid size for this case. With an 81×41 grid the residuals were still of the order of 10^{-3} after 2000 iterations, although the solution obtained with this grid was accurate. The reason for slow convergence with finer grids might be that the medium to long wavelength error components are being damped less effectively due to the decrease in numerical dissipation with mesh refinement.

The three-dimensional version of the code is implemented using a set of different preconditioning parameters γ and β^2 to solve for established flow in the quadrant of a square duct. A grid size of $21 \times 11 \times 11$ is used. An initial guess for (p, u, v, w) of (1, 1, 0, 0) was made. In Table 2 the number of iteration steps needed to achieve convergence are shown for several different test cases. Best results are obtained for cases 1 and 6. Case 6 corresponds to the pure artificial compressibility method and is chosen for later runs because of its simplicity.

Entry Flow

The three-dimensional version of the code was used to compute entry flow in a straight duct of square cross section at $Re = 32$ and $Re = 100$. The Reynolds number is based on the average velocity through the duct and the duct width. The calculations are carried out in a single quadrant of the duct due to symmetry.

The number of grid points in the streamwise, i.e., the x direction varies from 17 at a $Re = 32$ to 52 at a $Re = 100$ with a 9×9 grid in the other (i.e., y and z) directions. The grid spacing is somewhat nonuniform in the x direction close to the duct entrance but is uniform in the other two directions. At the entrance a plug flow profile is specified for the streamwise velocity component and the streamwise derivative of the remaining velocity components is set to zero. At the exit the streamwise derivative is assumed to vanish for all three velocity components.

Figures 2a–2c show the axial development of the computed as well as the measured normalized streamwise velocity component at the duct centerline. Figures 2a and 2b show the calculations at Reynolds numbers of 32 and 100, respectively, whereas Fig. 2c shows the calculation at a Reynolds number of 100, but for a computational domain shorter than that used for Fig. 2b. The experimental data were obtained from the laser Doppler velocimetry measurements of Goldstein and Kreid[13] for Reynolds numbers ranging between 69 and 387. As seen from these figures, the calculations agree with the experimental data. The shorter domain results shown in Fig. 2c do not differ from the results in Fig. 2b, indicating the effectiveness of a Neumann-type downstream boundary condition in minimizing the upstream influence on the flow. In Fig. 3 the velocity profiles at $x/(DRe) = 0.0075$ are given for both $Re = 32$ and $Re = 100$. The velocity profile corresponding to $Re = 100$ agrees better with the experimental results of Goldstein and Kreid. In Fig. 4 the same velocity profiles are given at $x/(DRe) = 0.02$. In this figure both velocity profiles agree with the experimental data. In Fig. 5 the computed pressure averaged over the cross-sectional area is compared with the experimental data of Beavers et al.[14] at $Re = 100$. Once again the agreement between calculations and the experimental data is good. The aforementioned test case results provide a measure of confidence in the ability of the code to accurately model the boundary-layer development in the entrance region of the duct.

Flow in a Bend

To verify the ability of the numerical procedure to model secondary flow phenomena accurately, flow in a 90-deg bend

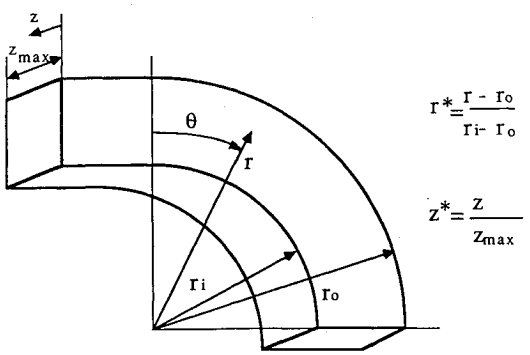

Fig. 6 Geometry of the 90-deg bend with square cross section.

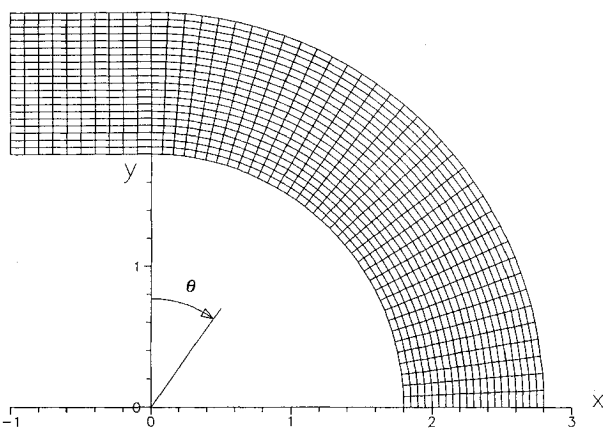

Fig. 7 Computational mesh at a z = const location of the bend.

with a mean radius that is a circular arc is solved. The cross section of the passage is square throughout the bend. The velocity and length scales used for nondimensionalization are the average entrance velocity and the entrance width. The Reynolds number based on these scales is 790. The mean radius of the bend is 2.3. A straight extension section (of length one) is attached upstream of the bend entrance. The primary reason for selecting the aforementioned geometrical parameters is to permit comparison with the experimental data of Taylor et al.[15] The parameters are such that the bend has a large enough turning angle and a small enough mean radius to generate severe distortion and significant secondary flow. The test case therefore is representative of the kind of problems one is likely to encounter in the context of oblique flow headers.

The flow geometry is shown in Fig. 6, and the computational mesh in the plane of the bend is shown in Fig. 7. The direction normal to the plane of the bend is defined by the z axis. Assuming symmetry in this direction, calculations are carried out only in the half width with z varying from 0.0 to 0.5. The discretization in the z direction is performed with uniform spacing between each of the z = const planes. The discretization within each of these planes is identical to that shown in Fig. 7.

At the entrance, an established flow profile is specified for the streamwise velocity component. The streamwise derivatives of the other two components at the entrance is assumed to vanish. This condition is also enforced at the downstream boundary for all three velocity components. The grid used for numerical results presented in this paper has 46 nodes in the streamwise direction with a 21×11 grid in the transverse plane. Note that the number of cells in the z direction is half that in the r direction because of symmetry. The individual control volumes are approximately cubical at the mean radius in the curved section. A sound speed β^2 of 3 for the Navier-Stokes equations is used. The unsteady form of the governing set of equations was iterated until the absolute maximum change in the pressure, as well as the velocity fields, was <0.00001. The coefficient for the fourth-order artificial dissipation ϵ is 0.05 and the implicit residual smoothing parameter in all three directions is 0.05.

Computational results are plotted in Figs. 8–10 along with the experimental data of Taylor et al.[15] The streamwise component of the velocity was the only component that we were able to recover from the rather tiny figures in their paper. Hence, this is the only component for which comparisons are shown. These data are available at three transverse planes of the bend, each plane being progressively downstream of the bend entrance. The measurement planes are defined using θ, an angular coordinate measured clockwise from the beginning of the curved portion of the bend. Data are available at $\theta = 30$, 60, and 77.5 deg. The planes $z = 0$ and $z = z_{max}$ correspond to the side wall and the plane $z = z_{max}/2$ corresponds to the centerplane. Approximately 10 data points equally spaced over the half-width are available in this direction. Nondimensional radial distance is defined as

$$r^* = (r_o - r)/(r_o - r_i) \tag{21}$$

where r_o and r_i are the outer and inner radii, respectively. Hence, $r^* = 1$ corresponds to the inner wall and $r^* = 0$ corresponds to the outer wall. Measurements provide data at five discrete r^* locations corresponding to 0.1, 0.3, 0.5, 0.7, and 0.9.

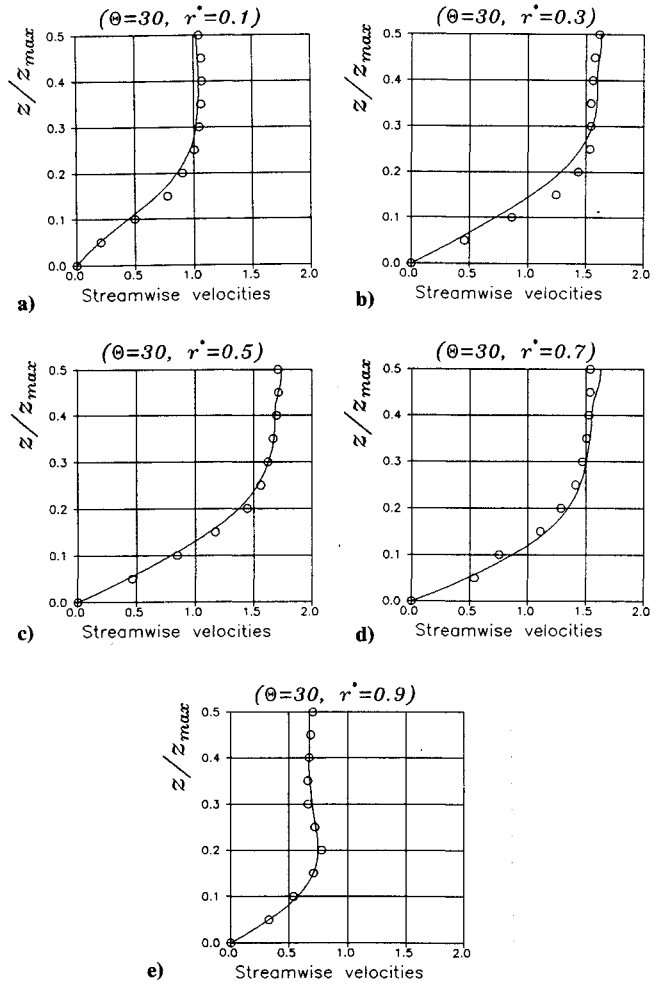

Fig. 8 Streamwise velocities in a bend at $\Theta = 30$ deg: a) $r^* = 0.1$; b) $r^* = 0.3$; c) $r^* = 0.5$; d) $r^* = 0.7$; e) $r^* = 0.9$.

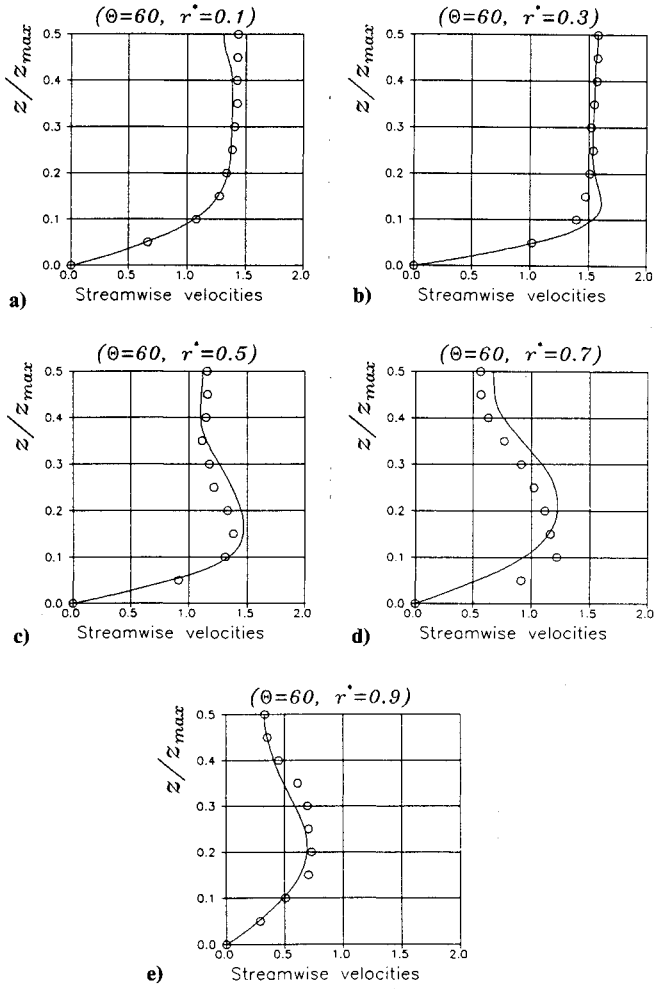

Fig. 9 Streamwise velocities in a bend at $\Theta = 60$ deg: a) $r^* = 0.1$; b) $r^* = 0.3$; c) $r^* = 0.5$; d) $r^* = 0.7$; e) $r^* = 0.9$.

Figures 8 and 9 shows particularly good agreement between the numerical results and the experimental data. Thus, the flow into about the first 60 deg of the curved portion of the bend is well modeled. The results at $\theta = 30$ deg show excellent agreement with the measured values. The velocity profile is still reminiscent of the fully developed flow upstream of the bend. As the flow proceeds farther into the bend, it begins to develop the characteristic skewness present in viscous flows negotiating a bend. The streamwise velocity is such that the bulk of the fluid is found progressively nearer the outer wall and along the side walls. This behavior is evidenced in the significantly higher velocities for r^* values of 0.1 and 0.3, as compared to 0.7 and 0.9. Note also the peak in the velocity profiles close to the side wall at about z/z_{max} of 0.2. The numerical results do show some difficulties in modeling the flow close to the side wall at $\theta = 77.5$ deg (see Fig. 10). The results suggest a need for additional grid points for accurate resolution of the flow gradients. A long, straight downstream section is present in the experiments of Taylor et al.,[15] which may influence the flow close to the exit of the curved passage. This may also contribute to the discrepancies between the computed velocities and the experimental data toward the exit of the bend.

Flow over Backward-Facing Step

Another problem that is examined is that of laminar flow in a channel between a flat wall and a wall with a backward-facing step. The geometry of the problem is shown in Fig. 11. The distance downstream of the step, l, is varied depending on the Reynolds number so that the exit boundary is sufficiently downstream of any possible region of flow reversal. This

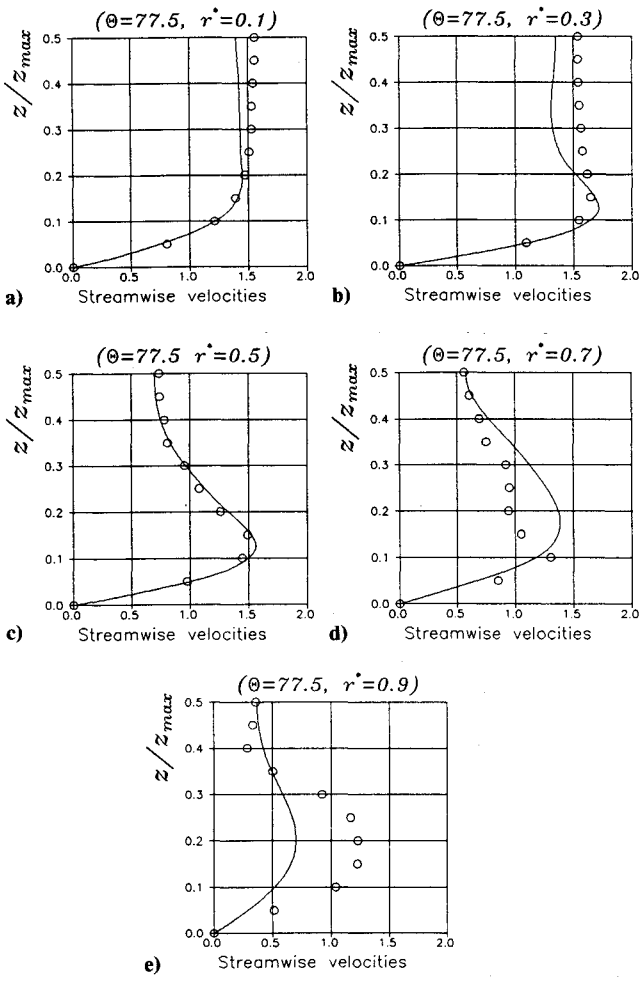

Fig. 10 Streamwise velocities in a bend at Θ = 77.5 deg: a) $r^* = 0.1$; b) $r^* = 0.3$; c) $r^* = 0.5$; d) $r^* = 0.7$; e) $r^* = 0.9$.

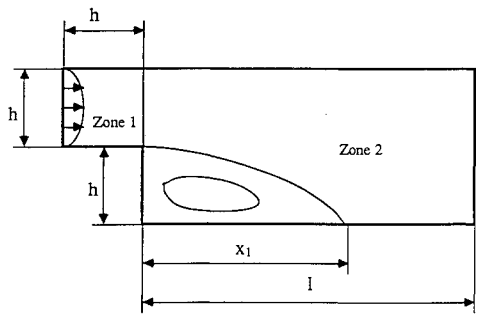

Fig. 11 Schematic diagram of a channel with a backward-facing step on the lower wall.

problem is a frequently utilized test case for Navier-Stokes code validation due to the presence of flow features such as flow detachment, recirculation, and flow reattachment. The Reynolds number is based on the mean velocity at the channel entrance and the step height. Calculations are carried out at several Reynolds numbers ranging from $Re = 50$ to $Re = 250$. The profile of the streamwise velocity at the upstream boundary is taken to be that of a fully developed channel flow. The streamwise derivative of the transverse velocity components at the entrance is set to zero. This condition is enforced at the downstream boundary as well for all the velocity components. The flow is assumed to be two dimensional.

The physical domain is divided into two rectangular computational subdomains, zone 1 and zone 2, as shown in Fig. 11. Each of the velocity components, pressure, and their first derivatives are matched at the zonal boundary between zones 1 and 2 at each iteration. The value of the dependent variables (u_i, p) at the zonal boundary is obtained as the mean of the cell centered values taken from cells adjoining the zonal boundary. The first derivative at the zonal boundary is obtained from a central difference procedure applied to the cell centered values. The grid spacing is $\Delta x = \Delta y = 0.1$ in both of the computational zones. This gave a grid size of 11×11 for zone 1. In zone 2, grid size along the y direction was 21. Grid size along the x direction was proportional to the length of the computational domain, which was chosen differently according to the Reynolds number. For example, at $Re = 50$, the grid size is 41×21 ($l = 4$), and at $Re = 250$, grid size was 121×21 ($l = 12$) in zone 2. A particular advantage of using this two zone approach for this problem is the ability to generate an orthogonal grid in each zone; thus, sharply distorted control volumes in the neighborhood of the step can be avoided.

The flow detaches at the edge of the backward-facing step and reattaches to the lower wall some distance x_1 downstream of the step. This distance is easily deduced from the computed velocity field and is also easily measured in an experiment. The quantity x_1 is normalized by the step height h, and the parameter x_1/h is plotted as a function of Reynolds numbers in Fig. 12. The figure also shows the computational results of Ku et al.[17] as well as the computational and experimental results of Armaly et al.[16] In Fig. 13, streamlines for $Re = 50$ are shown. Computed streamlines agree well qualitatively with the experimental observations.

The numerical results are found to be satisfactory, in general, at the Reynolds numbers considered in this study. At higher Reynolds numbers, the ability of the computations to model the flow accurately may deteriorate due to the following reasons: 1) longer computational domains are needed since the location of reattachment point moves downstream with increasing Reynolds number, 2) finer grids are needed to ensure solution resolutions, and 3) it may not suffice to assume that the flow is two dimensional. An attempt to satisfy the aforementioned requirements would increase the number of computational cells required dramatically. At Reynolds numbers greater than about 300, the difference in the location of the computed reattachment point and its experimental counterpart becomes greater than the channel height $2h$.

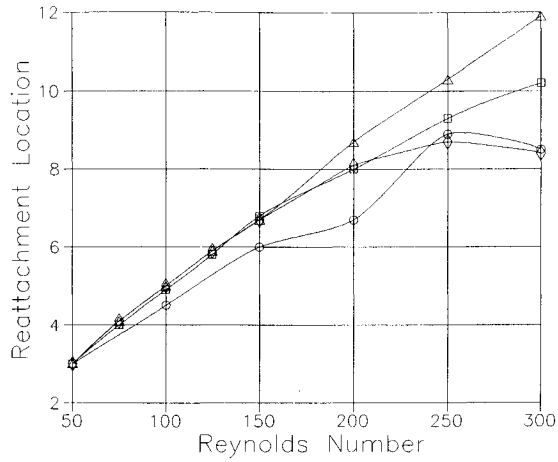

Fig. 12 Variation of the reattachment point, x_1/h, with Reynolds number: □, present computations; ○, data from Ref. 17 (numerical computations); ◇, data from Ref. 16 (numerical computations); Δ, data from Ref. 16 (experimental data).

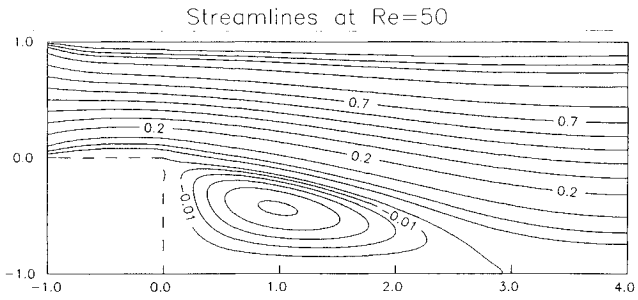

Fig. 13 Computed streamlines in a backward-facing step for a Reynolds number of 50 ($\psi_{min} = -0.051$).

Discussion and Conclusions

The steady incompressible laminar flow code was developed to carry out shape optimization of internal flow components. From the beginning it was desired that the code should be able to model features of internal flows accurately, such as boundary-layer development along the walls of the ducts, secondary flow effects in bends, and separating flows in diffuser-like geometries. The numerical experiments were chosen on the basis of the considerations previously discussed.

In general, it is found that the accuracy of the code agrees well with the experimental data available in the literature and the number of iterations needed for convergence were in the neighborhood of 1000. Even though some features such as local time stepping, preconditioning matrix method, and variable sound speed are included to reduce the number of iterations, these features are not fully optimized. In most of the test cases a constant sound speed (β^2) and zero preconditioning parameter (γ) have been employed. With these choices of sound speed and preconditioning parameter, the method essentially reduces to the pure artificial compressibility method.

The code is written for laminar flows, and solutions are obtained at Reynolds numbers less than 800. The CPU times for these calculations are of the order of few minutes on the Cray YMP for three-dimensional calculations and of the order of 1 h on an Intel 30836 based PC for the two-dimensional calculations. At higher Reynolds numbers finer grids would be needed to be able to model the smaller scales of the flows, thus increasing the computational task considerably.

Acknowledgments

The research reported in this paper is based upon work supported by the National Science Foundation under Grants CBT-87-10561, ASC-91-10514, and ASC-90-0027P. CHS would also like to acknowledge partial support from the Applied Hydrodynamics Research Program of the ONR. The authors also gratefully acknowledge the comments of William Smith of the David Taylor Research Center.

References

[1]Sung, C.-H., "Improvements in Incompressible Turbulent Horsoshoe Vortex Juncture Flow Calculations," AIAA Paper 91-0022, Jan. 1991.

[2]Chorin, A. J., "A Numerical Method for Solving Incompressible Viscous Flow Problems," *Journal of Computational Physics,* Vol. 2, No. 1, 1967, pp. 12–26.

[3]Yanenko, N. N., *The Method of Fractional Steps,* Springer-Verlag, New York, 1971; also, *Méthods a Pas Fractionnaires,* Armand Colin, Paris, 1968.

[4]Turkel, E., "Preconditioned Methods for Solving the Incompressible and Low Speed Compressible Equations," Inst. for Computer Applications in Science and Engineering, NASA Langley Research Center, Rept. 86-14, Hampton, VA, March 1986.

[5]Rizzi, A., and Eriksson, L.-E., "Computation of Inviscid Incompressible Flow with Rotation," *Journal of Fluid Mechanics,* Vol. 153, April 1985, pp. 275–312.

[6]Jameson, A., Schmidt, W., and Turkel, E., "Numerical Solutions of the Euler Equations by Finite Volume Methods Using Runge-Kutta Time-Stepping Schemes," AIAA Paper 81-1259, June 1981.

[7]Rizzi, A., and Eriksson, L.-E., "Computation of Flow Around Wings Based on the Euler Equations," *Journal of Fluid Mechanics,* Vol. 148, Nov. 1984, pp. 45–71.

[8]Grasso, F., Martinelli, L., and Jameson, A., "A Multistage Multigrid Method for the Compressible Navier-Stokes Equations," GAMM-Workshop on Numerical Simulation of Compressible Navier-Stokes Flows INRIA, Sophia Antipolis, France, 1985.

[9]Martinelli, L., "Calculation of Viscous Flows with a Multigrid Method," Ph.D. Dissertation, Dept. of Mechanical and Aerospace Engineering, Princeton Univ., Princeton, NJ, Oct. 1987.

[10]Swanson, R. C., and Turkel, E., "A Multistage Time-Stepping Scheme for the Navier-Stokes Equations," AIAA Paper 85-35, Jan. 1985.

[11]Vatsa, V. N., "Accurate Solutions for Transonic Viscous Flow Over Finite Wings," AIAA Paper 86-1052, May 1986.

[12]Sung, C.-H., "An Explicit Runge-Kutta Method for Three-Dimensional Turbulent Incompressible Flows," David W. Taylor Naval Ship Research and Development Center, Ship Hydromechanics Dept. Rept. DTNSRDC/SHD-1244-01, Bethesda, MD, 1987.

[13]Goldstein, R. J., and Kreid, D. K., "Measurement of Laminar Flow Development in a Square Duct Using a Laser-Doppler Flowmeter," *Journal of Applied Mechanics, Series E,* Vol. 89, No. 4, 1967, pp. 813–818.

[14]Beavers, G. S., Sparrow, E. M., and Magnuson, R. A., "Experiments on Hydrodynamically Developing Flow in Rectangular Ducts of Arbitrary Aspect Ratio," *International Journal of Heat and Mass Transfer,* Vol. 13, No. 4, 1970, pp. 689–702.

[15]Taylor, A. M. K. P., Whitelaw, J. H., and Yianneskis, M., "Curved Ducts With Strong Secondary Motion: Velocity Measurements of Developing Laminar and Turbulent Flow," *Journal of Fluids Engineering,* Vol. 104, No. 3, 1982, pp. 350–359.

[16]Armaly, B. F., Durst, F., Pereira, J. C. F., and Schönung, "Experimental and Theoretical Investigation of Backward-Facing Step Bow," *Journal of Fluid Mechanics,* Vol. 127, Feb. 1983, pp. 473–496.

[17]Ku, H. C., Hirsh, R. S., Taylor, T. D., and Rosenberg, A. P., "A Pseudospectral Matrix Element Method for Solution of Three-dimensional Incompressible Flows and its Parallel Implementation," *Journal of Computational Physics,* Vol. 83, No. 2, 1989, pp. 260–291.

[18]Van der Houwen, P. J., *Construction of Integration Formulas for Initial Value Problems,* North-Holland, Amsterdam, 1977.

[19]Pike, J., and Roe, P. L., "Accelerated Convergence of Jameson's Finite-Volume Euler Scheme Using van der Houwen Integrations," *Computers and Fluids,* Vol. 13, No. 2, 1985, pp. 223–236.

[20]Swanson, R. C., and Turkel, E., "Pseudo-Time Algorithm for the Navier-Stokes Equations," Inst. for Computer Applications in Science and Engineering, NASA Langley Research Center, Rept. 8637, Hampton, VA, May 1986.

[21]Crocco, L., "A Suggestion for the Numerical Solution of the Steady Navier-Stokes Equations," *AIAA Journal,* Vol. 3, No. 10, 1965, pp. 1824–1832.

[22]Jameson, A., "Numerical Solutions of the Euler Equation for Compressible Inviscid Fluids," *Numerical Methods for the Euler Equations of Fluid Dynamics,* edited by F. Angrand and A. Dervieux, Society of Industrial and Applied Mathematics, Philadelphia, PA, 1985, pp. 191–245.